oxidation peak assignable to the cyclopentadienide, possibly because the solvent (THF) oxidizes the reduced ferrocene before it decomplexes. In contrast, **14** was expected to be more easily reducible, but the attempted dehydration of **11** (with heat, catalytic acid, or 2,4-dinitrobenzenesulfenyl chloride) in each case gave a mixture of products, none of which showed an NMR spectrum suggestive of the desired structure of **14**.

The bromo ketal **3** was also tested as a precursor to a C_5-substituted ferrocene similar to **11** (Scheme V). The product would be more easily reduced, as it contains the acetyl group. However, reaction of the lithiated ketal[26] with 2-cyclopenten-1-one followed by hydrolysis gave only acetylferrocene, probably because the ketone acts as an acid.

Conclusions

In this paper we report electrochemical evidence for the formation of the new heterobimetallic complex **1** (M = $W(CO)_3^-$, M′ = $Fe(CO)_2^-$) by reduction of **6**. Decomplexation of the ferrocene unit in **6** occurs in low yield, and pinacol dimers are the major product of the reduction. The overall synthesis of **1** can be made easier (four steps) by using a more direct route to **4** starting with commercially available chloromercuriferrocene.[16,19] One advantage of the method is that several of the intermediates are air-stable solids which allows relatively simple handling procedures.

The reaction conditions involved in the decomplexation reaction are relatively mild so that weakly coordinated or unstable ligands could have been incorporated into the final product. A limitation of the method is that the metal to be attached first (i.e., in compound **6**) must be stable to the reducing conditions required for the next step. We do not feel this is a restrictive limitation.

As described above, the yield of **1** prepared from **4** is limited by the side reactions to form pinacols. Although outside the scope of the present study, we feel that the use of a sterically demanding group such as *t*-Bu or Si(*t*-Bu)$_3$ attached to the ketone could be explored to block this side reaction. This would require the synthesis of the diacylated analogue of **4** for which the starting materials involved are less available. Cyano-based analogues of **4** might also be available in reasonable yield from biferrocenyl and may behave more favorably.

If the radical anion of C_5-substituted ferrocenes can be made inert to side reactions, decoordination of the ferrocene unit may occur in reasonable yield. This would open a useful synthetic pathway to new heterobimetallic complexes containing the fulvalene molecule.

Acknowledgment. The support of the National Science Foundation (CHE8402135) is gratefully acknowledged. We also wish to thank Dr. C. Wilcox for his help in planning the syntheses.

Registry No. **2**, 12088-99-2; **3**, 111291-37-3; lithiated **3**, 111291-42-0; debrominated **3**, 42086-47-5; **4**, 12203-92-8; **5**, 111291-38-4; **6**, 111291-39-5; H_2-**9** (R = CH_3, R′ = H), 55351-91-2; **11**, 111291-41-9; $W(CO)_3(PrCN)_3$, 83732-34-7; (acetylCp)$W(CO)_3CH_3$, 73249-59-9; ((1′-acetylferrocenyl)Cp)$W(CO)_3I$, 111291-40-8; ethylene glycol, 107-21-1; ethylene dibromide, 106-93-4; acetylferrocene, 1271-55-2; 1,1′-dilithioferrocenebis(tetramethylethylenediamine), 65587-59-9; 2-cyclopenten-1-one, 930-30-3.

(26) Rausch, M. D.; Moser, G. A.; Meade, C. F. *J. Org. Chem.* **1973**, *51*, 1.

Electrochemical Behavior of Thiolate-Bridged Manganese Dimers

Leslie J. Lyons,[1a] Marvin H. Tegen,[1a] Kenneth J. Haller,[1a] Dennis H. Evans,[1b]* and Paul M. Treichel*[1a]

Department of Chemistry, University of Wisconsin—Madison, Madison, Wisconsin 53706, and Department of Chemistry and Biochemistry, University of Delaware, Newark, Delaware 19716

Received June 4, 1987

The oxidative behavior of thiolate-bridged manganese dimers having the general formulae $Et_4N[Mn_2(\mu\text{-}SR)_3(CO)_6]$, $Mn_2(\mu\text{-}SR)_2L_2(CO)_6$, and $Mn_2(\mu\text{-}SR)_2(\mu\text{-}CO)L_2(CO)_4$ where R = Me, *t*-Bu, or Ph and L = PMe_3, PPh_3, or $CH_2[PPh_2]_2$ (dppm) was studied. The ease of oxidation is dependent on the electron-donating ability of the R group in the thiolate bridge of the dimers. Oxidation of a recently characterized compound, $Mn_2(\mu\text{-}SMe)_2(\mu\text{-}CO)(PMe_3)_2(CO)_4$, occurs by an ECE (E = electrochemical step, C = chemical step) process. The character of the chemical step has been probed by cyclic voltammetry in solvents of varying donor ability and through ESR spectroscopy of the intermediate. The ECE mechanism has been confirmed quantitatively by digital simulation. An X-ray structure determination was carried out on $Mn_2(\mu\text{-}SMe)_2(\mu\text{-}CO)(PMe_3)_2(CO)_4$. Crystal data: monoclinic, space group $P2_1/c$; a = 9.753 (4), b = 14.872 (6), c = 16.052 (6) Å; β = 115.38 (2)°; Z = 4. The Mn–Mn distance is 2.581 Å, and the bridging carbonyl is symmetrically disposed with respect to the two manganese atoms.

Introduction

Studies on the oxidation and reduction chemistry of organometallic compounds have been greatly advanced by the availability of information from electrochemical experiments. In the past few years, there has been extensive integration of chemical and electrochemical experiments using organometallic complexes. Such studies have produced, notably, information on the tendencies toward oxidation or reduction as a function of the type of com-

(1) (a) University of Wisconsin. (b) University of Delaware.

0276-7333/88/2307-0357$01.50/0

pound or ligand.[2] Upon oxidation or reduction of organometallic complexes one often encounters isomerization processes; here electrochemical techniques have provided valuable kinetic and thermodynamic information that explains descriptive chemical information.[3] The redox behavior of metal cluster species has been another major area of study.[4] For such species redox processes are often accompanied by structural modifications of the cluster. Cluster species have been, of course, very much in the forefront of interest due to potential catalytic activity of such species. Finally, one may note the use of electrochemical synthetic procedures[5] and electrochemical catalytic processes.[6] Such procedures can be quite valuable tools for the synthetic chemist.

Metal complexes having bridging thiolate ligands have frequently been subjects of electrochemical investigation. Most often, these investigations have been carried out in conjunction with synthetic procedures designed to isolate and characterize two or more members of a series of complexes having the same stoichiometry but different net charges. When isolation of several members of such a series of compounds has proven possible, the determination of molecular structure of each has usually been undertaken. Often, it has been found that there are bond length and bond angle changes which accompany oxidation or reduction, such changes being indicative of a change in metal–metal bond order.[7]

The project described in this paper combines synthetic and electrochemical skills of two research groups in an ongoing project involving manganese carbonyl thiolate complexes.[8] In this paper, the electrochemical behavior of three different types of compounds is described. The general formulae for these species are $Et_4N[Mn_2(\mu\text{-}SR)_3(CO)_6]$ (I), $Mn_2(\mu\text{-}SR)_2L_2(CO)_6$ (II), and $Mn_2(\mu\text{-}SR)_2(\mu\text{-}CO)L_2(CO)_4$ (III); structures of these species are represented below. There has been little previous electrochemistry reported on manganese thiolate species. However, the electrochemistry of a complex of type I has been described in the literature.[9] We also describe the structural characterization of one complex of type III by X-ray crystallography.

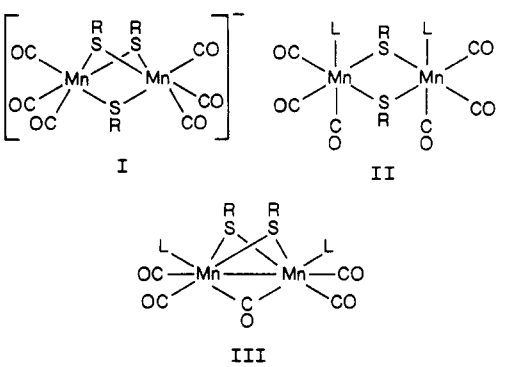

I

II

III

Experimental Section

Electrochemistry. Tetrabutylammonium perchlorate (TBAP) was purchased from Southwestern Analytical and vacuum dried at 60 °C before using. In all experiments, 0.10 M TBAP was used as the supporting electrolyte in the respective solvents. High-purity acetonitrile (UV grade) and methylene chloride were purchased from Burdick and Jackson (Muskegon, MI) and were used as received. Other solvents were commercial grade and were distilled immediately prior to use. Acetone and nitromethane were distilled by using standard methods, and propylene carbonate was dried over anhydrous copper sulfate and vacuum distilled. The purified solvent was stored over dry molecular sieves (type 3a).

Electrochemical measurements were made by using a Princeton Applied Research (EG&G Princeton Applied Research, Princeton, NJ) PAR Model 175 signal generator and a PAR Model 173 three-electrode potentiostat equipped with a PAR Model 176 current-to-voltage converter. Solution resistance was compensated by using the positive feedback resistance compensation circuit of the 176. The amount of resistance to be compensated was determined in two ways. First, the solution resistance between the circular platinum disk working electrode (0.125-cm radius) and a distance counter electrode was calculated by using the expression $R = \rho/4r$ where ρ is the resistivity of the solution and r is the radius of the working electrode.[10] For 0.10 M TBAP solutions in methylene chloride, ρ has been reported[11] to be 725 Ω cm and, in acetonitrile, it is 132 Ω-cm. These values lead to calculated resistances between the working electrode and a distant counter electrode of 1450 and 264 Ω, respectively. The tip of the reference electrode probe was positioned at a distance equal to about four radii from the center of the working electrode so that the effective solution resistance between working and reference will be about 85% of the total resistance[10] or about 1200 Ω for methylene chloride and 220 Ω for acetonitrile.

In the second method, oxidation of ferrocene was studied by cyclic voltammetry using two solvents (acetonitrile and methylene chloride). The resistance compensation was adjusted so that the anodic-to-cathodic peak potential separation remained close to the reversible limit over a range of scan rates (0.2–2 V/s in methylene chloride and 0.2–20 V/s in acetonitrile) and a range of concentrations (1.0–10 mM in methylene chloride). The required compensation was 1250 ± 100 Ω in methylene chloride and 190 Ω in acetonitrile. These values were close to those which induce oscillation in the circuit.

From the above measurements, it is concluded that the solution resistance was adequately compensated with a residual uncertainty of about 100 Ω in methylene chloride and 30 Ω in acetonitrile. These values led to maximum errors in the potential (at the highest currents observed) of about 40 and 9 mV, respectively.

The voltammetric data were collected with a Nicolet Model 4094 digital oscilloscope and transferred to an IBM Model 9000 computer for analysis. Background voltammograms were obtained in separate experiments with solvent and supporting electrolyte, and these were subtracted from the raw data to provide background-corrected voltammograms. All data reported in this paper have been corrected in this way.

The cell for voltammetry was of standard design[12] and included inlet ports for the working electrode, counter electrode (platinum wire), and reference electrode probe. The reference electrode was an aqueous saturated calomel electrode (SCE), and the closure of the probe tip was a cracked glass seal. The stability of the SCE was verified by frequent measurement of the reversible half-wave potential for the ferrocene 0/+ couple. In acetonitrile the value was +0.39 V vs SCE. In acetone and methylene chloride the

(2) (a) Holland, G. F.; Ellis, D. E.; Trogler, W. C. *J. Am. Chem. Soc.* **1986**, *108*, 1884. (b) Bursten, B. E. *J. Am. Chem. Soc.* **1982**, *104*, 1299. (c) Treichel, P. M.; Mueh, H. J.; Bursten, B. E. *J. Organomet. Chem.* **1976**, *110*, C49. (d) Lloyd, M. K.; McCleverty, J. A.; Connor, J. A.; Jones, E. M. *J. Chem. Soc., Dalton Trans.* **1973**, 1768. (e) Frisch, P. D.; Lloyd, M. K.; McCleverty, J. A.; Seddon, D. *J. Chem. Soc., Dalton Trans.* **1973**, 2268.

(3) Evans, D. H.; O'Connell, K. M. In *Electroanalytical Chemistry*; Bard, A. J., Ed.; Marcel Dekker: New York, 1986; Vol. 14, pp 112–207.

(4) Geiger, W. E.; Connelly, N. G. In *Advances in Organometallic Chemistry*; Academic: New York, 1985; Vol. 24, pp 111–122.

(5) Nagy, Z. *Electrochemical Synthesis of Inorganic Compounds*; Plenum: New York, 1985.

(6) Narayanan, B. A.; Amatore, C.; Kochi, J. K. *Organometallics* **1987**, *6*, 129 and references therein.

(7) Bedard, R. L.; Dahl, L. F. *J. Am. Chem. Soc.* **1986**, *108*, 5942.

(8) (a) Treichel, P. M.; Tegen, M. H. *J. Organomet. Chem.* **1985**, *292*, 385. (b) Treichel, P. M.; Nakagaki, P. C. *Organometallics* **1986**, *5*, 711.

(9) McDonald, J. W. *Inorg. Chem.* **1985**, *24*, 1734.

(10) Newman, J. *J. Electrochem. Soc.* **1966**, *113*, 501.

(11) Kadish, K. M.; Ding, J. Q.; Malinski, T. *Anal. Chem.* **1984**, *56*, 1741.

(12) Evans, D. H.; Jimenez, P. J.; Kelly, M. J. *J. Electroanal. Chem.* **1984**, *163*, 145.

half-wave potential was 0.53 V vs SCE and 0.48 V vs SCE, respectively. The solution temperature was ambient (22 ± 2 °C).

The working electrode was a platinum disk (diameter = 0.25 cm) sealed in soft glass which was polished on a polishing wheel with 0.3 μm alumina followed by 0.05 μm alumina. The electrode was then rinsed in a sonicating bath with triply distilled water and further rinsed with the electrochemical solvent. This process yielded a reproducible surface for all experiments.

Digital simulations were performed by using the explicit finite difference method of Feldberg.[13] The experimental data were obtained for the oxidation of $Mn_2(\mu\text{-}SMe)_2(\mu\text{-}CO)(PMe_3)_2(CO)_4$ which was postulated to undergo an ECE-type mechanism. In this shorthand representation, E indicates an electron-transfer reaction occurring at the electrode surface and C indicates a chemical reaction proceeding in solution near the electrode. The overall process is outlined in Scheme III. The starting material, A, is oxidized to a cation, A^+, which is thought to be attacked by a molecule of solvent (acetonitrile) to open the CO bridge with addition of acetonitrile to one of the manganese centers. This chemical step was treated as an irreversible reaction in the simulation. The resulting "open" cation, B^+, is also electroactive so it loses another electron to give a dication, B^{2+}. This is the ECE sequence mentioned above. In addition, allowance is made for the oxidation of A^+ at a more positive potential to give A^{2+} which reacts very rapidly with acetonitrile to produce B^{2+}. These two steps were combined and treated as a totally irreversible electrode reaction in the simulation; i.e., the rate of A^+ oxidation was derived from a heterogeneous electron-transfer rate constant, transfer coefficient, and surface concentration, and the flux of B^{2+} leaving the electrode surface was set equal and opposite to the flux of A^+ consumed.

Both the A/A^+ and B^+/B^{2+} couples are treated as relatively reversible reactions, but the B/B^+ couple was treated in two different ways. The voltammetric results suggested that when the neutral "open" compound, B, was formed on the return sweep, it lost acetonitrile very rapidly with restoration of the CO bridge giving the starting material, A. For scan rates of 50 V/s or less, the B^+/B to A sequence was combined into a single irreversible electrode reaction ($B^+ + e \rightarrow A$) just as was done for the oxidation of A^+ to B^{2+}. For scan rates exceeding 50 V/s, the B to A reaction was not complete so it was simulated as an irreversible chemical reaction in the normal way.

In complex reaction schemes, it is necessary to consider various electron-transfer reactions which can occur in solution near the electrode among the members of the scheme. Depending upon the details of the reaction scheme, these reactions can affect the voltammetric response in a significant way. In this case there are six species involved. Of these six, both A^{2+} and B are thought to have very short lifetimes so their concentrations are never very large. The remaining four can participate in reaction 1. Solution

$$B^+ + A^+ \rightarrow B^{2+} + A \quad (1)$$

electron-transfer reactions involving little structural change are very rapid, so reaction 1 was simulated as a fast reaction that remained close to equilibrium. The equilibrium constant of reaction 1 is not adjustable as it is dictated by the standard potentials chosen for the A/A^+ and B^+/B^{2+} couples.

The simulations assumed linear diffusion and equal diffusion coefficients for all species. The stepsize was 2.57 mV per time unit when parameters were being optimized. Once the best values of the parameters had been chosen, a simulation was repeated with a 1 mV stepsize to confirm that no significant changes occurred.

Electron Spin Resonance Spectroscopy. ESR spectra were recorded on a Varian Model E15 spectrometer at variable temperatures using a Varian Model 4343 variable-temperature controller. The microwave power ranged from 0.1 to 30 mW, and spectra were recorded over a 1000-G range. A rectangular cavity (Waveline Type 674-10) held the electrolysis cell and variable-temperature jacket. Measurements of the hyperfine coupling (A) and g value were calculated by using diphenylpicrylhydrazyl (DPPH) as a standard. Microwave frequencies were determined with an Hewlett-Packard Model 5257A transfer oscillator and Hewlett-Packard Model 5245L electronic counter to sample the frequencies. Oxidized species were generated in situ by placing gold electrodes in the ESR cell and electrolyzing the sample with a Heath transistorized power supply while observing the ESR signal. The ESR cell used in this experiment has been previously described.[14] The electrodes were constructed from 0.5-mm diameter gold wire. The cathode was a straight gold wire while the anode was a 4.5-cm helix surrounding the cathode and positioned close to the inner wall of the cell. The two electrodes were separated by Teflon tubing to prevent electrical shorting. In this way, the maximum amount of oxidized material was generated near the cell wall in the cavity where the sensitivity is greatest. The ESR signal was measured while currents ranging from 20 to 50 μA were generated.

Synthesis. The synthesis of the $Et_4N[Mn_2(\mu\text{-}SR)_3(CO)_6]$ complexes and their reactions to produce $cis\text{-}Mn_2(\mu\text{-}SR)_2L_2(CO)_6$ have been recently described.[8] The preparation of the carbonyl-bridged complexes from the thermal conversion of $cis\text{-}Mn_2(\mu\text{-}SR)_2(PR_3)_2(CO)_6$ is one synthetic route described in the previously cited paper. A direct synthesis is described here.

Synthesis of $Mn_2(\mu\text{-}SR)_2(\mu\text{-}CO)(PMe_3)_2(CO)_4$ (R = Me, Ph, t-Bu). A solution of 1.0 g (2 mmol) of $Mn_2(\mu\text{-}SR)_2(CO)_8$ and 0.6 mL (5.8 mmol) of PMe_3 in 50 mL of THF was refluxed for 2 h (R = Me, Ph) or 4 h (R = t-Bu). The dark solutions were evaporated to dryness, and the product was recrystallized from CH_2Cl_2/hexane. Purification by chromatography on alumina gave analytically pure compounds.

$Mn_2(\mu\text{-}SMe)_2(\mu\text{-}CO)(PMe_3)_2(CO)_4$: dark red; yield 0.81 g (82%); mp 235 °C; mass spectrum peak match found 495.9302, calcd 495.9297; ^1H NMR ($CDCl_3$) δ 1.62 (d, intensity 6, J_{PH} = 7.1 Hz), 1.67 (s, intensity 3); IR ($CHCl_3$) ν(CO) 1982 s, 1941 s, 1898 s, 1803 w, br cm^{-1}. Anal. Calcd for $C_{13}H_{24}O_5P_2S_2Mn_2$: C, 31.32; H, 4.86. Found: C, 31.62; H, 4.93.

$Mn_2(\mu\text{-}SPh)_2(\mu\text{-}CO)(PMe_3)_2(CO)_4$: dark purple; yield 1.05 g (85%); mp 164–165 °C; ^1H NMR ($CDCl_3$) δ 1.56 (d, intensity 9, J_{PH} = 7.8 Hz), 7.17 (m, intensity 3), 7.35 (m, intensity 2); IR ($CHCl_3$) ν(CO) 1985 s, 1947 s, 1905 m, 1805 w, br cm^{-1}. Anal. Calcd for $C_{23}H_{28}O_5P_2S_2Mn_2$: C, 44.51; H, 4.55. Found: C, 44.091; H, 4.89.

$Mn_2(\mu\text{-}SBu)_2(\mu\text{-}CO)(PMe_3)_2(CO)_4$: dark red, yield 0.79 g (68%) mp 200 °C dec; mass spectrum found 580.0242, calcd for $C_{19}H_{36}O_5P_2S_2Mn_2$ 580.0233; ^1H NMR ($CDCl_3$) δ 1.32 (s, intensity 1), 1.51 (d, intensity 1, J_{PH} = 6.2 Hz); IR ($CHCl_3$) ν(CO) 1978 s, 1937 s, 1896, m, 1802 w, br cm^{-1}.

Synthesis of $Mn_2(\mu\text{-}SR)_2(\mu\text{-}CO)(PPh_3)_2(CO)_4$ (R = Me, Ph). A solution of 0.6 g (1.0 mmol) of $MnBr(PPh_3)_2(CO)_3$ and 0.5 mL (1.5 mmol) of n-Bu_3SnSR in 50 mL of THF was refluxed for 3 h. After cooling, the dark reaction mixture was evaporated to dryness and redissolved in CH_2Cl_2. Addition of hexane and cooling (−15 °C) caused formation of dark crystals.

$Mn_2(\mu\text{-}SMe)_2(\mu\text{-}CO)(PPh_3)_2(CO)_4$: dark red; yield 0.44 g (51%); mp >250 °C; IR ($CHCl_3$) ν(CO) 1984 s, 1947 s, 1905 s, 1810 w, br cm^{-1}; ^1H NMR ($CDCl_3$) δ 1.85 (s, intensity 1), 7.16 (m), 7.35 (m, intensity 5). Anal. Calcd for $C_{43}H_{36}O_5P_2S_2Mn_2$: C, 59.45; H, 4.18. Found: C, 59.23; H, 4.30.

$Mn_2(\mu\text{-}SPh)_2(\mu\text{-}CO)(PPh_3)_2(CO)_4$: black: yield 0.46 g (46%); mp 158 °C; IR ($CHCl_3$) ν(CO) 1988 s, 1953 s, 1912 m, 1810 w, br cm^{-1}. ^1H NMR ($CDCl_3$) δ 7.18 (m, intensity 2), 7.38 (m, intensity 3). Anal. Calcd for $C_{53}H_{40}O_5P_2S_2Mn_2$: C, 64.12; H, 4.06. Found: C, 64.31; H, 4.23.

X-ray Diffraction Study of $Mn_2(\mu\text{-}SMe)_2(\mu\text{-}CO)(PMe_3)_2(CO)_4$. Dark red crystals suitable for diffraction were obtained from methylene chloride/hexane solution at −15 °C. A single crystal, attached to a glass fiber with cyanoacrylate glue, was mounted on a Syntex-Nicolet P1 diffractometer equipped with a graphite-monochromated Mo Kα radiation source ($\lambda_{MoK\alpha}$ = 0.71073 Å). The diffraction experiment procedures closely parallel those reported earlier.[15] The crystal was of fairly equant habit so an absorption correction was not applied. Crystal data are

(13) Feldberg, S. W. In *Electroanalytical Chemistry*; Bard, A. J., Ed.; Marcel Dekker: New York, 1969; Vol. 3, pp 199–296.

(14) (a) Ohya-Nishiguchi, H. *Bull. Chem. Soc. Jpn.* **1979**, *52*, 2064. (b) Allendoerfer, R.; Martinchek, G. A.; Bruckenstein, S. *Anal. Chem.* **1975**, *47*, 890.

(15) Haller, K. J.; Enemark, J. H. *Inorg. Chem.* **1978**, *17*, 3552.

Table I. Summary of Crystal Data and Intensity Collection

empirical formula	$Mn_2S_2P_2O_5C_{13}H_{24}$
fw	496.3
cryst dimens, mm	0.5 × 0.6 × 0.7
temp, K	202 (±5)
cell parameters	
a, Å	9.753 (4)
b, Å	14.872 (6)
c, Å	16.052 (6)
β, deg	115.38 (2)
space group	$P2_1/c$ (No. 14)
Z	4
D(calcd), g/cm^3	1.56
absorpt coeff, μ, cm^{-1}	14.8
scan range	
deg below 2θ(Mo Kα$_1$)	0.75
deg above 2θ(Mo Kα$_2$)	0.75
scan speed, deg/min	3.43–24.0
scan type (bisecting geometry)	θ–2θ
2θ limits, deg (±*h*,+*k*,+l)	3.5–56.8
(sin θ)/λ$_{max}$, Å^{-1}	0.669
unique data	
measd	5307
$F_o > 3\sigma(F_o)$	4479
p; weight = $(\sigma^2(F_o) + (pF_o)^2)^{-1/2}$	0.04
discrepancy indices	
R_1	0.039
R_2	0.053
goodness of fit	1.73
observn/variable ratio	14.3

Table II. Fractional Monoclinic Coordinates for $Mn_2(\mu\text{-SMe})_2(\mu\text{-CO})(PMe_3)_2(CO)_4$

atom	*x*	*y*	*z*	*B*(iso), Å^2
Mn(1)	0.46956 (4)	0.215200 (26)	0.361824 (28)	1.26
Mn(2)	0.24189 (4)	0.321381 (27)	0.326212 (27)	1.21
S(1)	0.38117 (8)	0.25671 (5)	0.46993 (5)	1.69
S(2)	0.49002 (7)	0.37155 (5)	0.37117 (5)	1.58
C(1)	0.5370 (3)	0.20294 (20)	0.27445 (21)	1.96
O(1)	0.5773 (3)	0.19520 (19)	0.21710 (18)	2.85
C(2)	0.4306 (3)	0.09876 (20)	0.36818 (22)	1.96
O(2)	0.4047 (3)	0.02385 (15)	0.37389 (20)	2.93
P(1)	0.71237 (8)	0.18863 (5)	0.46639 (5)	1.57
C(3)	0.7958 (4)	0.08780 (25)	0.44366 (28)	2.58
C(4)	0.7419 (4)	0.17501 (26)	0.58553 (23)	2.25
C(5)	0.8509 (4)	0.27369 (24)	0.47435 (25)	2.28
C(6)	0.2684 (3)	0.21660 (19)	0.25371 (20)	1.72
O(6)	0.19752 (25)	0.17901 (15)	0.18414 (15)	2.20
C(7)	0.2811 (5)	0.16539 (28)	0.4951 (3)	2.58
C(8)	0.5156 (4)	0.41983 (25)	0.27446 (27)	2.33
C(9)	0.0689 (3)	0.26466 (20)	0.30795 (20)	1.74
O(9)	−0.03879 (25)	0.22511 (16)	0.29646 (17)	2.50
C(10)	0.16955 (29)	0.37499 (19)	0.21658 (20)	1.62
O(10)	0.12319 (24)	0.40926 (16)	0.14451 (15)	2.32
P(2)	0.16660 (8)	0.44473 (5)	0.37831 (5)	1.61
C(11)	0.2001 (5)	0.44423 (24)	0.49893 (24)	2.29
C(12)	0.2524 (5)	0.54985 (23)	0.36745 (29)	2.55
C(13)	−0.0351 (4)	0.46930 (27)	0.3187 (3)	2.94
H(3A)	0.914 (5)	0.082 (3)	0.493 (3)	5.2 (11)
H(3B)	0.732 (4)	0.0307 (26)	0.4414 (28)	3.0 (8)
H(3C)	0.775 (6)	0.081 (4)	0.377 (4)	6.8 (14)
H(4A)	0.841 (4)	0.1609 (23)	0.6206 (24)	1.9 (7)
H(4B)	0.683 (5)	0.1300 (29)	0.5584 (29)	3.8 (9)
H(4C)	0.711 (5)	0.2272 (28)	0.6027 (29)	3.6 (9)
H(5A)	0.817 (4)	0.3353 (27)	0.4830 (27)	3.2 (8)
H(5B)	0.941 (5)	0.262 (3)	0.520 (3)	3.7 (9)
H(5C)	0.852 (5)	0.270 (3)	0.414 (3)	4.7 (11)
H(7A)	0.351 (5)	0.124 (3)	0.538 (3)	4.5 (10)
H(7B)	0.203 (4)	0.1249 (26)	0.435 (3)	3.4 (9)
H(7C)	0.225 (6)	0.185 (3)	0.518 (4)	5.4 (13)
H(8A)	0.453 (4)	0.3905 (23)	0.2157 (26)	2.1 (7)

[a] The estimated standard deviations of the least significant digits are given in parentheses. [b] Equivalent isotropic thermal parameters are given for the atoms that were refined anisotropically.

summarized in Table I. The structure was solved by Patterson and difference electron density Fourier syntheses and was refined by using full-matrix least-squares techniques[16] (EFFT 80 Fourier summation; RAELS least-squares refinement, distance/angle, and error calculations; and ORTEP molecular diagrams running on a Harris/7 computer). Parameters varied in the final cycles of the least-squares refinement included positions and anisotropic thermal parameters for all non-hydrogen atoms and positions and isotropic thermal parameters for all hydrogen atoms. Fractional monoclinic coordinates and isotropic thermal parameters are tabulated in Table II. Selected interatomic distances and angles are given in Table III. Anisotropic thermal parameters, more complete lists of interatomic distances and angles, and a listing of $10F_o$ and $10F_c$ are given in the supplementary material.

Table III. Interatomic Distances and Angles for $Mn_2(\mu\text{-SMe})_2(\mu\text{-CO})(PMe_3)_2(CO)_4$

Distances (Å)			
Mn(1)–Mn(2)	2.581 (1)	Mn(1)–S(1)	2.328 (1)
Mn(1)–S(2)	2.333 (1)	Mn(1)–C(1)	1.795 (3)
Mn(1)–C(2)	1.785 (3)	Mn(1)–P(1)	2.274 (1)
Mn(1)–C(6)	1.985 (3)	Mn(2)–S(1)	2.325 (1)
Mn(2)–S(2)	2.332 (1)	Mn(2)–C(6)	2.027 (3)
Mn(2)–C(9)	1.794 (3)	Mn(2)–C(10)	1.779 (3)
Mn(2)–P(2)	2.265 (1)	S(1)–C(7)	1.816 (4)
S(2)–C(8)	1.822 (3)	C(1)–O(1)	1.151 (4)
C(2)–O(2)	1.155 (4)	P(1)–C(3)	1.816 (3)
P(1)–C(4)	1.819 (3)	P(1)–C(5)	1.815 (3)
C(6)–O(6)	1.173 (3)	C(9)–O(9)	1.148 (3)
C(10)–O(10)	1.164 (3)	P(2)–C(11)	1.820 (3)
P(2)–C(12)	1.817 (4)	P(2)–C(13)	1.818 (4)
Angles (deg)			
Mn(2)–Mn(1)–S(1)	56.25 (2)	Mn(2)–Mn(1)–S(2)	56.37 (2)
Mn(2)–Mn(1)–C(1)	117.23 (9)	Mn(2)–Mn(1)–C(2)	114.97 (10)
Mn(2)–Mn(1)–P(1)	142.59 (3)	Mn(2)–Mn(1)–C(6)	50.67 (8)
S(1)–Mn(1)–S(2)	74.72 (3)	S(1)–Mn(1)–C(1)	170.41 (10)
S(1)–Mn(1)–C(2)	93.36 (10)	S(1)–Mn(1)–P(1)	95.57 (3)
S(1)–Mn(1)–C(6)	96.08 (8)	S(2)–Mn(1)–C(1)	95.83 (10)
S(2)–Mn(1)–C(2)	167.83 (10)	S(2)–Mn(1)–P(1)	95.30 (3)
S(2)–Mn(1)–C(6)	94.07 (8)	C(1)–Mn(1)–C(2)	95.99 (14)
C(1)–Mn(1)–P(1)	86.83 (10)	C(1)–Mn(1)–C(6)	82.75 (12)
C(2)–Mn(1)–P(1)	88.23 (10)	C(2)–Mn(1)–C(6)	84.57 (13)
P(1)–Mn(1)–C(6)	166.63 (9)	Mn(1)–Mn(2)–S(1)	56.36 (2)
Mn(1)–Mn(2)–S(2)	56.44 (2)	Mn(1)–Mn(2)–C(6)	49.25 (8)
Mn(1)–Mn(2)–C(9)	114.06 (10)	Mn(1)–Mn(2)–C(10)	115.58 (9)
Mn(1)–Mn(2)–P(2)	142.94 (3)	S(1)–Mn(2)–S(2)	74.81 (3)
S(1)–Mn(2)–C(6)	95.02 (9)	Sn(1)–Mn(2)–C(9)	94.36 (10)
S(1)–Mn(2)–C(10)	169.13 (9)	S(1)–Mn(2)–P(2)	96.47 (3)
S(2)–Mn(2)–C(6)	93.02 (8)	S(2)–Mn(2)–C(9)	168.35 (10)
S(2)–Mn(2)–C(10)	94.68 (9)	S(2)–Mn(2)–P(2)	94.84 (3)
C(6)–Mn(2)–C(9)	83.52 (12)	C(6)–Mn(2)–C(10)	82.57 (13)
C(6)–Mn(2)–P(2)	167.45 (9)	C(9)–Mn(2)–C(10)	95.90 (13)
C(9)–Mn(2)–P(2)	90.59 (10)	C(10)–Mn(2)–P(2)	87.05 (9)
Mn(1)–S(1)–Mn(1)	67.39 (2)	Mn(1)–S(1)–C(7)	111.93 (15)
Mn(2)–S(1)–C(7)	112.91 (14)	Mn(1)–S(2)–Mn(2)	67.19 (2)
Mn(1)–S(2)–C(8)	112.16 (13)	Mn(2)–S(2)–C(8)	111.44 (12)
Mn(1)–C(6)–Mn(2)	80.08 (11)	Mn(1)–C(6)–O(6)	141.78 (23)
Mn(2)–C(6)–O(6)	138.14 (23)	Mn(1)–C(6)–O(6)	141.78 (23)
Mn(2)–C(6)–O(6)	138.14 (23)		

Results and Discussion

$Et_4N[Mn_2(\mu\text{-SR})_3(CO)_6]$. The synthetic routes and mechanisms for these compounds have been described recently.[8] The synthesis can be summarized as

$$\underset{\substack{M = Bu_3Sn,\ Na\\ M = H}}{Mn(CO)_5Cl \text{ or } Mn_2(\mu\text{-Cl})_2(CO)_8} + \underset{\substack{R = t\text{-Bu, Me, Ph}\\ R = Ph,\ t\text{-Bu}}}{MSR} \rightarrow Et_4N[Mn_2(\mu\text{-SR})_3(CO)_6]$$

$$[Mn(CO)_5]^- + F_3CSSCF_3 \rightarrow [Mn_2(\mu\text{-SCF}_3)_3(CO)_6]^-$$

The focus on this paper is the voltammetric behavior observed. The oxidation of each of the four compounds in this series occurs by two one-electron processes in sequence to give the neutral and monocation products. Cyclic voltammetric data are summarized in Table IV.

(16) Atomic form factors from: Cramer, D. T.; Mann, J. B. *International Tables for X-Ray Crystallography*; Kynoch: Birmingham, England, 1974.

Table IV. Cyclic Voltammetric Data[a]

compound	couple	$E_{1/2}$,[b] V	ΔE_p,[c] mV	i_{pc}/i_{pa}
$Et_4N[Mn_2(\mu\text{-}SMe)_3(CO)_6]$	1−/0	0.185	87	1.00
	0/1+	0.595	63	1.02
$Et_4N[Mn_2(\mu\text{-}S\text{-}t\text{-}Bu)_3(CO)_6]$	1−/0	0.225	53	0.94
	0/1+	0.668	94	1.02
$Et_4N[Mn_2(\mu\text{-}SPh)_3(CO)_6]$	1−/0	0.380	67	1.06
		0.52[d]		
	0/1+	0.755	55	1.09
		0.82[d]		
$Et_4N[Mn_2(\mu\text{-}SCF_3)_3(CO)_6]$	1−/0	0.966	56	1.05
	0/1+	1.430	72	0.92
$Mn_2(\mu\text{-}SMe)_2(dppm)(CO)_6$	0/1+	0.672	58	0.93
	1+/2+	0.972	63	0.91
$Mn_2(\mu\text{-}S\text{-}t\text{-}Bu)_2(PMe_3)_2(CO)_6$	0/1+	0.700	52	0.79
	1+/2+	1.094	202	0.78
$Mn_2(\mu\text{-}S\text{-}t\text{-}Bu)_2(dppm)(CO)_6$	0/1+	0.742	66	0.71
	1+/2+	1.011	90	0.75
$Mn_2(\mu\text{-}SPh)_2(dppm)(CO)_6$	0/1+	0.851	64	0.77
	1+/2+	1.119	56	1.00

[a] 0.10 M TBAP in acetonitrile. Platinum disk working electrode. Scan rate = 0.200 V/s. [b] V vs SCE. Reversible half-wave potential taken as mean of anodic and cathodic peak potentials. [c] Anodic peak potential minus cathodic peak potential. [d] In DMF, −45 °C.[9]

The electrode reactions are quasi-reversible. The separations of the anodic and cathodic peaks at 200 mV/s are close to the reversible limit (57 mV[17]) for most of the couples, but the separation increases at faster scan rates for all of the reactions as expected for the onset of rate control by heterogeneous electron transfer kinetics. The peak separation for ferrocene oxidation under the same conditions remained near the reversible limit as the scan rate was varied (see Experimental Section), attesting to the fact that the increased separations for the manganese compounds were not caused by uncompensated solution resistance. Both the neutral and monocation product appear to be stable on the voltammetric time scale as evidenced by the ratios of cathodic to anodic peak currents which were close to unity for all couples (Table IV).

For processes having the characteristics described above, the mean of the anodic and cathodic peak potentials is a good measure of the reversible half-wave potential, $E_{1/2}$, of the reaction which in turn is almost equal to the reversible formal potential of the redox couple.[18]

The values of $E_{1/2}$ are sensitive to the identity of R, with complexes having electron-donating methyl and *tert*-butyl groups being most easily oxidized and the electron-withdrawing trifluoromethyl derivative having the most positive $E_{1/2}$. This sensitivity to the electronic properties of R indicates that the HOMO from which electrons are removed has a significant amount of thiolate character. The $E_{1/2}$ for the neutral/cation couple is about 0.4 V more positive than that of the anion/neutral couple for each compound. Separations of this magnitude are commonly seen in cases where two electrons are successively removed from (or added to) a molecule.

One cannot deduce structural information directly from the electrochemical data, but on the basis of the EAN rule and analogy to other compounds, we propose that the oxidation of these anions is accompanied by an increase in bond order between the manganese atoms. In the neutral species a delocalized interaction between the manganese atoms (bond order = $^1/_2$) occurs, and in the cation a metal–metal bond is proposed (Scheme I). Recently, McDonald reported the electrochemical behavior of the phenyl derivative and the ESR spectrum for the chemically generated $Mn_2(\mu\text{-}SPh)_3(CO)_6$, the product of a one electron oxidation.[9] He obtained an 11-line pattern with a hyperfine coupling constant of 33 G. The ESR spectrum indicates the interaction of the unpaired electron with two equivalent manganese nuclei which is consistent with the formulation in Scheme I.

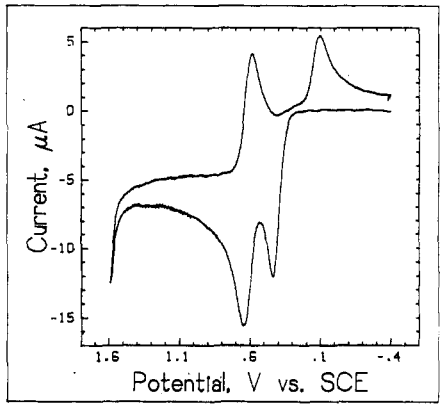

Figure 1. Cyclic voltammogram of 1.0 mM $Mn_2(\mu\text{-}SPh)_2(dppm)(CO)_6$ in 0.10 M TBAP/acetonitrile at 0.200 V/s.

Scheme I. Oxidation of $Et_4N[Mn_2(\mu\text{-}SR)_3(CO)_6]$

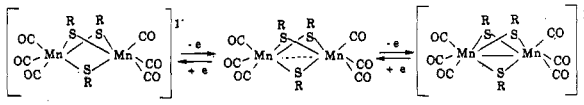

***cis*-$Mn_2(\mu\text{-}SR)_2L_2(CO)_6$.** Phosphine-substituted thiolate-bridged metal dimers have been known since 1968.[19] They have been assigned a cis arrangement of the noncarbonyl ligands on the basis of their having five carbonyl bands in their IR spectra (e.g. $Mn_2(\mu\text{-}SMe)_2(PMe_3)_2(CO)_6$: ν 2020 s, 1995 s, 1936 m, 1910 s, 1900 s cm^{-1}) as would be expected for compounds having C_{2v} symmetry.

It is reasonable to predict that molecules with a cis arrangement of ligands, L, should be less stable than the trans due to greater steric interaction of these ligands. Supporting this contention, Kullmer and Vahrenkamp[20] have reported that the compound *cis*-$Re_2(\mu\text{-}SH)_2(PMe_3)_2(CO)_6$ converts to the trans isomer upon recrystallization in benzene. In fact the compounds once reported to be *trans*-$Mn_2(\mu\text{-}SR)_2(PPh_3)_2(CO)_6$ (R = *p*-tolyl, Me)[19] actually have a different stoichiometry and structure; we will comment on this later.

The electrochemical oxidation of these compounds is similar to that of the triply thiolate-bridged anions. The neutral compound is oxidized in two quasi-reversible one-electron steps. The voltammogram for $Mn_2(\mu\text{-}SPh)_2(dppm)(CO)_6$ (Figure 1) is representative of the general behavior. Cyclic voltammetric data are summarized in Table IV.

There is evidence that some of the monocation and dication products upon oxidation may decompose on the time scale of voltammetry, as indicated by peak current ratios less than unity. Also, the second oxidation process of $Mn_2(\mu\text{-}S\text{-}t\text{-}Bu)_2(PMe_3)_2(CO)_6$ appears to have a somewhat smaller electron-transfer rate constant than the other reactions as indicated by the large peak separation. In general, however, the reactions can be described adequately as the simple stepwise oxidation, first to the monocation and then to the dication.

(17) Bard, A. J.; Faulkner, L. R. *Electrochemical Methods: Fundamental and Applications*; Wiley: New York, 1980; p 230.

(18) For the process $O + ne \rightarrow R$, $E_{1/2} = E^{o\prime} - (RT/2F) \ln (D_O/D_R)$ where $E^{o\prime}$ is the reversible formal potential and D_O and D_R are the diffusion coefficients of O and R, respectively. Often the term involving the diffusion coefficients does not exceed a few millivolts.

(19) Abel, E. W.; Atkins, A. M.; Crosse, B. C.; Hutson, G. V. *J. Chem. Soc. A* **1968**, 647.

(20) Kullmer, V.; Vahrenkamp, H. *Chem. Ber.* **1977**, *110*, 3799.

Scheme II. Oxidation of $Mn_2(\mu\text{-}SR)_2L_2(CO)_6$

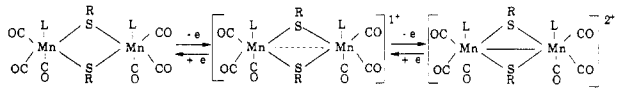

As was seen with the triply thiolate-bridged anions, the values of $E_{1/2}$ become progressively more positive along the series of the Me, *t*-Bu, and Ph derivatives (with the common phosphine ligand, dppm) and the shift in $E_{1/2}$ from one derivative to the next is about the same. Again, as in the tris(thiolato)-bridged anions, the anomalous reversal of the *t*-Bu and Me derivatives is observed, wherein the compounds with the more strongly electron-donating butyl group are actually more difficult to oxidize than the corresponding Me compounds. This difference is small but reproducible. The reversal may be of steric origin or associated with solvation effects on the starting material and/or products.

In this series of bis(thiolato)-bridged dimers, the $E_{1/2}$ for the second oxidation is 0.3–0.4 V positive of that for the first. In the one case where a comparison can be made ($Mn_2(\mu\text{-S-}t\text{-Bu})_2(dppm)(CO)_6$ vs $Mn_2(\mu\text{-S-}t\text{-Bu})_2(PMe_3)_2(CO)_6$) a change in the phosphine ligand was found to have little effect (<0.1 V) on the values of $E_{1/2}$. This suggests that the HOMO energy is much more sensitive to the electronic properties of the bridging thiolates than it is to the other ligands. Fenske–Hall molecular orbital calculations[21] verify that the phosphine ligands play a small role in the character of the HOMO. The HOMO is 75% metal and 25% thiolate in character and is influenced only slightly by the phosphine ligands which contribute to the metal portion of the HOMO.

We expect that oxidation of these compounds increases the bond order between the manganese atoms (Scheme II). Teo et al.[22] in a theoretical study on $Mn_2(CO)_8(\mu\text{-}PH_2)_2$ predicted an increase in Mn–Mn bond order upon oxidation. From that study and the 18-electron rule, we predict the existence of a metal–metal bond in the dication.

$Mn_2(\mu\text{-}SR)_2(\mu\text{-}CO)L_2(CO)_4$. Compounds of the type $M_2(\mu\text{-}SR)_2(\mu\text{-}CO)(PR'_3)_2(CO)_4$ have been known for nearly 20 years, but they were incorrectly characterized in their initial report by Abel and co-workers.[19] In 1968, these researchers reported the synthesis of a dark red complex from the reactions of $MnBr(PPh_3)_2(CO)_3$ and Me_3SnSR (R = Tol, Me), which on the basis of IR and elemental analyses, were assigned the formulae *trans*-$Mn_2(\mu\text{-}SMe)_2(PPh_3)_2(CO)_6$ (ν(CO) 1979 s, 1946 s, 1904 s cm^{-1}) and *trans*-$Mn_2(\mu\text{-S-p-}C_6H_4CH_3)_2(PPh_3)_2(CO)_6$ (ν(CO) 1982 s, 1952 s, 1910 s cm^{-1}), respectively. The trans assignment was made on symmetry arguments based on the number of CO bands. A complex with trans geometry of the phosphine ligands with respect to the Mn_2S_2 plane would have C_{2h} symmetry, and thus three CO bands ($A_u + 2B_u$) would be expected.

A reexamination of the IR spectra reported for the compounds by Abel et al. indicated not only the carbonyl bands at 1984 s, 1947 s, and 1905 m cm^{-1} as had been reported but also a very weak band at 1810 cm^{-1}. A cyclic voltammogram of the compound $Mn_2(\mu\text{-}SMe)_2(\mu\text{-}CO)(PMe_3)_2(CO)_4$ (prepared according to ref 20) showed identical behavior to that of Abel and co-workers' compound. From the similarities in their color, IR spectra, and cyclic voltammetric behavior, we felt that the compounds previously designated as trans isomers of $Mn_2(\mu\text{-}SR)_2L_2(CO)_6$ were in fact compounds of the same structural type as reported by Kullmer and Vahrenkamp, namely, those with a bridging carbonyl. Elemental analyses, obtained by us, of the compounds synthesized according to Abel's procedure were in agreement with the values reported in the literature. Both our analysis and Abel's set of values were closer to the calculated values for $Mn_2(\mu\text{-}SR)_2(\mu\text{-}CO)(PMe_3)_2(CO)_4$ than those calculated for $Mn_2(\mu\text{-}SR)_2(PMe_3)_2(CO)_6$, but since the difference in the two compounds is the presence of one carbonyl group, the two sets of calculated values differ by less than 1.0%.

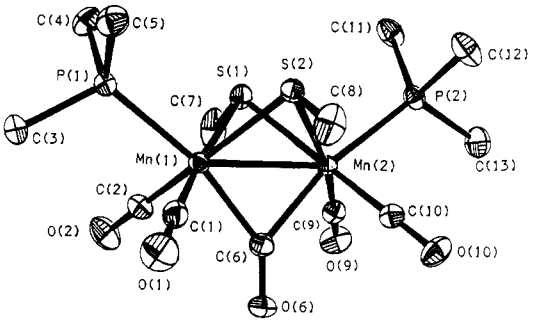

Figure 2. ORTEP diagram of $Mn_2(\mu\text{-}SMe)_2(\mu\text{-}CO)(PMe_3)_2(CO)_4$. Thermal ellipsoids are drawn at 50% probability.

In 1977, Kullmer and Vahrenkamp[20] found that *cis*-$Mn_2(\mu\text{-}SMe)_2(PMe_3)_2(CO)_6$ (R = H, CH_3, $SnMe_3$) would readily lose CO to yield dark red complexes having the formula $Mn_2(\mu\text{-}SMe)_2(\mu\text{-}CO)(PMe_3)_2(CO)_4$. This structural assignment was made on the basis of IR and elemental analysis data. Although the similar compounds $Mn_2(\mu\text{-}NC(CF_3)_2)_2(\mu\text{-}CO)(CO)_6$[23] and $Mn_2(\mu\text{-}PPh_2)_2(\mu\text{-}CO)(CO)_6$[24] have been reported in the literature, the formation of $Mn_2(\mu\text{-}SR)_2(\mu\text{-}CO)(PR'_3)_2(CO)_4$ via loss of CO was unexpected. Whereas in the references cited above the parent compounds contained eight terminal CO ligands and thus one might expect the carbonyls to be labile, the loss of CO from the octacarbonyl complex had been accomplished only by photolysis or prolonged heating. The compounds $Mn_2(\mu\text{-}SR)_2(PR'_3)_2(CO)_6$ might be expected to be less susceptible to CO loss due to increase electron density on the metal by virtue of the replacement of two CO ligands by phosphines; instead they lose 1 equiv of CO readily at room temperature in solution.

After the experimental evidence was examined, it becomes apparent that steric factors are much more important than electronic factors in explaining these results. In the octacarbonyl complexes mentioned earlier, $Mn_2(\mu\text{-}PPh_2)_2(CO)_8$ and $Mn_2(\mu\text{-}NC(CF_3)_2)_2(CO)_8$, there is no steric interaction between the carbonyl groups and so, even if a CO dissociates, it can readily reassociate with the metal. Only when forcing conditions are used to completely remove the CO does a second CO bridge and a metal–metal bond form. This is not the case when two CO's have been replaced by phosphine ligands. When cis phosphines are present, their steric requirements distort the M_2S_2 from the planarity of the octacarbonyl case to a more crowded structure with the phosphines pointing away from the metals. In the phosphine-substituted case the loss of one of the CO ligands would relieve steric strain in the molecule.

In order to retain an 18-electron configuration about each metal upon CO loss, formation of a metal–metal bond must occur along with the incorporation of a terminal CO

(21) Kanis, D., personal communication.
(22) Teo, B. K.; Hall, M. B.; Fenske, R. F.; Dahl, L. F. *J. Organomet. Chem.* **1974**, *70*, 413.
(23) Churchill, M. R.; Lin, K. G. *Inorg. Chem.* **1975**, *14*, 1675.
(24) Kawamura, T.; Sowa, T.; Yonezawa, T.; Yamabe, T. *J. Organomet. Chem.* **1984**, *276*, C10.

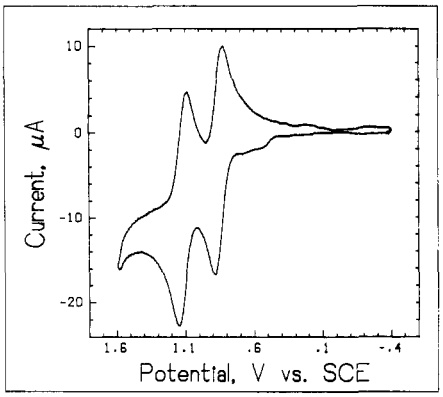

Figure 3. Cyclic voltammogram of 1.0 mM $Mn_2(\mu\text{-}SMe)_2(\mu\text{-}CO)(PMe_3)_2(CO)_4$ in 0.10 M TBAP/acetonitrile at 0.200 V/s.

Table V. Cyclic Voltammetric Data for $Mn_2(\mu\text{-}SR)_2(\mu\text{-}CO)(PR_3)_2(CO)_4$[a]

compound	peak potential, V vs SCE: oxidation			reduction	
$Mn_2(\mu\text{-}SMe)_2(\mu\text{-}CO)(PPh_3)_2(CO)_4$	0.482	0.696		0.156	0.646
$Mn_2(\mu\text{-}SMe)_2(\mu\text{-}CO)(PMe_3)_2(CO)_4$	0.511	0.690		0.171	0.620
$Mn_2(\mu\text{-}SPh)_2(\mu\text{-}CO)(PMe_3)_2(CO)_4$	0.450			[b]	
$Mn_2(\mu\text{-}SBu^t)_2(\mu\text{-}CO)(PMe_3)_2(CO)_4$	0.626	0.958		[b]	
$Mn_2(\mu\text{-}SPh)_2(\mu\text{-}CO)(PPh_3)_2(CO)_4$	0.662	0.926	1.479	[b]	

[a] 0.10 M TBAP in acetonitrile. Platinum disk working electrode. Scan rate = 0.200 V/s. [b] No reduction peaks.

in the bridging position. Both of these features are evident in the X-ray structure of $Mn_2(\mu\text{-}SMe)_2(\mu\text{-}CO)(PMe_3)_2(CO)_4$ (Figure 2). The geometry around the manganese atoms is essentially octahedral with the bridging carbonyl trans to the phosphine ligands. The Mn–Mn distance is 2.581 Å (Table III), a value indicative of a metal–metal bond and significantly shorter than the Mn–Mn distance in the triply thiolate-bridged anion $[Mn_2(\mu\text{-}SPh)_3(CO)_6]^-$ (3.238 Å).[25] From the similarity of the angles formed between the manganese atoms and the bridging sulfur or carbon (see Table III) the symmetry of the bridging groups is apparent. In this compound the bridging carbonyl is bound symmetrically to both metal centers.

The voltammetric behavior of this series of compounds differs markedly from that of the compounds discussed earlier. A cyclic voltammogram of $Mn_2(\mu\text{-}SMe)_2(\mu\text{-}CO)(PMe_3)_2(CO)_4$ in acetonitrile at a scan rate of 0.2 V/s is shown in Figure 3. Two anodic peaks are observed, and their heights are approximately equal as would be found for the stepwise oxidation to the cation and dication. There is a reduction peak at about +0.6 V (vs SCE) which may be associated with the second oxidation peak at about +0.7 V. Another reduction peak is observed at +0.1 V, but it is displaced about 0.4 V from the first oxidation peak, and there is no assurance that it is associated in any way with the first oxidation process. Both reduction peaks are similar in height to the two oxidation peaks as would be expected if the oxidation products were reducible at the electrode.

Five compounds in this series were investigated, and the voltammetric data are summarized in Table V. The two

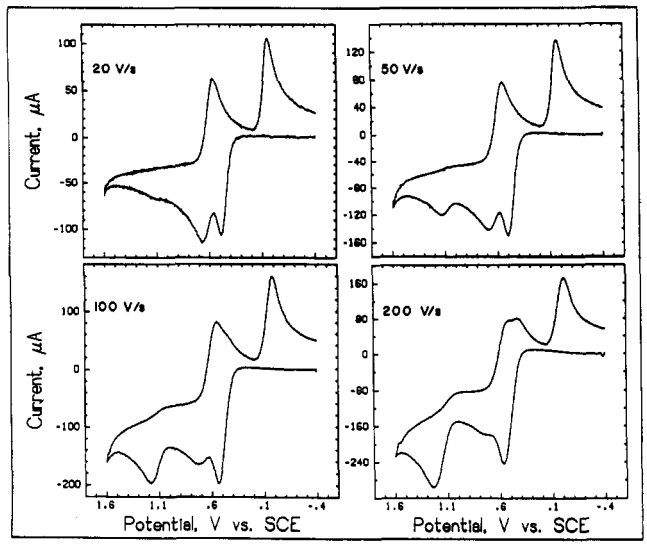

Figure 4. Cyclic voltammograms of 1.0 mM $Mn_2(\mu\text{-}SMe)_2(\mu\text{-}CO)(PMe_3)_2(CO)_4$ in 0.10 M TBAP/acetonitrile at several faster scan rates.

Scheme III. ECE Process for Oxidation of $Mn_2(\mu\text{-}SMe)_2(\mu\text{-}CO)(PMe_3)_2(CO)_4$ in Acetonitrile Solvent

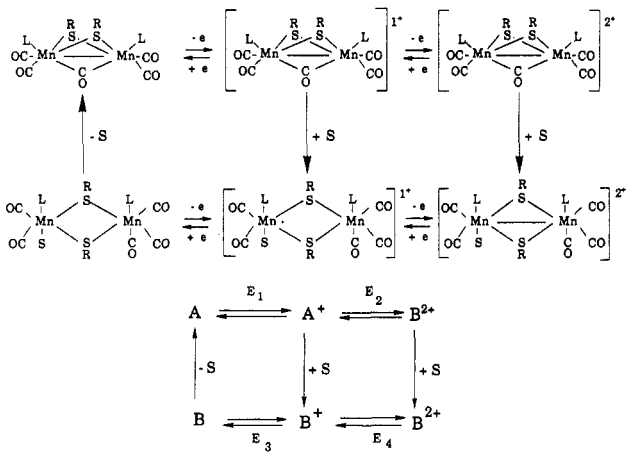

compounds with SMe bridges give qualitatively similar voltammograms, but when the thiolate bridge is SPh or S-*t*-Bu, the oxidation peaks are totally irreversible; apparently the cationic products of the electrode reactions react rapidly to give substances which are not reducible in the potential range investigated.

In order to gain more information about the oxidative behavior of $Mn_2(\mu\text{-}SMe)_2(\mu\text{-}CO)(PMe_3)_2(CO)_4$, voltammetric data at higher scan rates were obtained (Figure 4). Though a number of changes are evident, the most striking is the waning of the oxidation peak at +0.7 V and the appearance and growth of a new oxidation peak at about +1.2 V as the scan rate was increased. At the fastest scan rate shown, the residue of the +0.7 V peak is still discernible, but it disappears altogether at about 1000 V/s. This behavior suggests that an ECE process is occurring.[26] The product of the oxidation at the first anodic peak undergoes a chemical reaction to form a new species which is oxidized a second time at the +0.7-V anodic peak. When the time scale of the experiment is short, this chemical reaction does not reach completion and the peak at +0.7 V becomes small and eventually disappears in the fastest experiments. At that limit, the initially formed product of the first

(25) Tegen, M. H. Ph.D. Thesis, University of Wisconsin, Madison, WI, 1985.

(26) In this notation the E refers to an electrode reaction and the C signifies a chemical reaction occurring near the electrode surface.

oxidation process can be detected through its oxidation at about +1.2 V.

The proposed ECE reaction scheme is given in Scheme III in both molecular and schematic forms. The electrochemical data do not provide direct structural information about the intermediates and products in the scheme, so it is necessary to postulate structures. Chemical and spectroscopic evidence supporting these assignments will be presented in the next section.

It is reasonable to suppose that the primary oxidation at about +0.4 V and the peak at +1.2 V seen at fast scan rates correspond to oxidation of $Mn_2(\mu\text{-}SMe)_2(\mu\text{-}CO)(PMe_3)_2(CO)_4$, called A for simplicity, to the cation, A^+, and dication, A^{2+}, of the CO-bridged species. Fenske–Hall calculations performed on the neutral dimer, A, do not clearly indicate the character of the HOMO in this compound since both metal bonding and antibonding orbitals are quite close in energy. As a result, the effect of oxidation on the metal–metal bond is uncertain. The calculation and an analysis of the bonding will be discussed in a forthcoming publication.[27]

We propose that the chemical step in the ECE mechanism is the coordination of a solvent molecule (acetonitrile) to A^+ with displacement of the bridging carbonyl to a terminal position. The resulting dithiolate-bridged cation, B^+, is more easily oxidized than A^+ and produces the oxidation peak at about +0.7 V which is prominent at low scan rates (Figure 3). Other features are required to account for the qualitative shape of the voltammograms. The A^{2+} formed at +1.2 V must react quickly (no return peak for the reduction of A^{2+} is seen at any scan rate). The B^{2+} persists even at the slowest scan rate and produces the prominent reduction peak near +0.6 V, and, finally, the postulated neutral species, B, reacts rapidly as shown by the fact that no peak for the oxidation of B to B^+ is seen on the second positive-going scan at scan rates less than 200 V/s. It is significant to note that B, B^+, and B^{2+} are analogous to compounds of type II and their proposed behavior mirrors Scheme II.

We sought to determine if the voltammetric results could be quantitatively accounted for by Scheme III. Digital simulations were fit to the voltammograms obtained at 10, 20, 50, and 100 V/s; it was found that quite adequate agreement was obtained at each scan rate using constant values of the adjustable parameters in Scheme III. Interestingly, it proved to be impossible to obtain acceptable agreement between simulation and experiment unless an important solution electron transfer reaction was included. This solution reaction (reaction 1, Experimental Section) is

$$B^+ + A^+ \rightarrow B^{2+} + A$$

No significant structural change accompanies this reaction so it is not surprising that it is fast enough to remain close to equilibrium in our experiments. Reaction 1 was treated as a perfectly mobile reaction with an equilibrium constant (4.3×10^{-3}) dictated by the values of the formal potentials chosen for the simulations. The effect is illustrated in Figure 5 which shows simulations of the 50 V/s voltammogram without (Figure 5A) and with (Figure 5B) reaction 1. We conclude that Scheme III provides an adequate quantitative description of the overall electrode reaction. The greatest deviation between simulation and experiment occurs at potentials positive of the A^+/A^{2+} oxidation peak where we apparently are unable to completely correct the voltammograms for the background capacitive current.

(27) Kanis, D.; Fenske, R. F., manuscript in preparation.

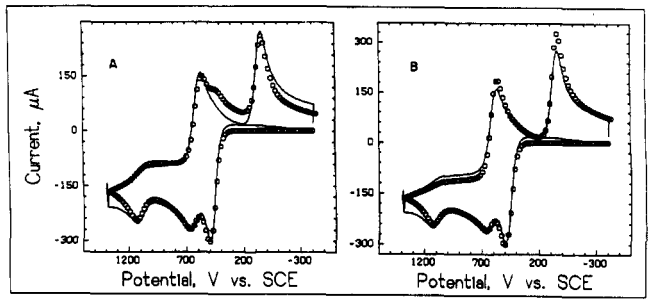

Figure 5. Comparison of digital simulation (points) with experimental cyclic voltammogram of 0.95 mM $Mn_2(\mu\text{-}SMe)_2(\mu\text{-}CO)(PMe_3)_2(CO)_4$ in 0.10 M TBAP/acetonitrile at 50 V/s: A, simulation without solution electron transfer reaction 1; B, simulation including reaction 1.

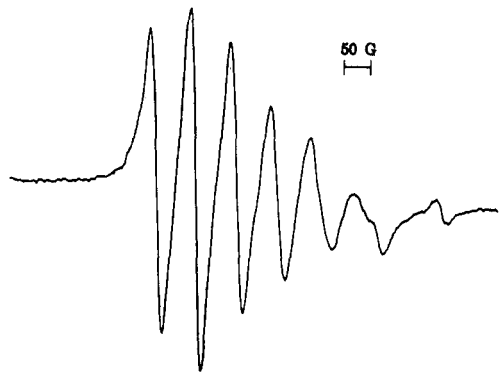

Figure 6. ESR spectrum obtained upon anodic oxidation of $Mn_2(\mu\text{-}SMe)_2(\mu\text{-}CO)(PMe_3)_2(CO)_4$ in 0.10 M TBAP/acetonitrile at 241 K.

In the simulations, the values of the formal potentials were +0.490, +0.630, and +0.050 V for the A^+/A, B^{2+}/B^+, and B^+/B couples, respectively. The rate constant for the coordination of acetonitrile ($A^+ \rightarrow B^+$) required to match the data was 210 s^{-1}. Preliminary simulations of fast scan rate data (300 and 400 V/s) indicate that reformation of the CO bridge with expulsion of acetonitrile in the neutral species ($B \rightarrow A$) occurs with a rate constant of about 600 s^{-1}.

Several pieces of experimental evidence support the chemical reaction proposed in Scheme III. The most conclusive evidence would be the structural characterization of the product formed by electrolysis at about +0.55 V (B^+) or that formed at >+0.7 V (B^{2+}). Unfortunately, in our hands these species proved to be too unstable to isolate. However, several results can be cited that support the solvent addition proposed in Scheme III. First, the fact that the product of the chemical reaction, B^+, is more easily oxidized than A^+ is consistent with the coordination of a species like acetonitrile which is a better donor ligand than CO. Secondly, the electrochemically generated cation produced a six-line ESR spectrum with a hyperfine coupling constant of 55 G (Figure 6). This is consistent with an unsymmetrical dimanganese cation such as B^+ in which splitting by only one manganese nucleus occurs. Finally, we removed acetonitrile as a reactant by studing the electrochemical oxidation in acetone, nitromethane, propylene carbonate, and dichloromethane (Figure 7) as solvents. Each of these solvents has poorer ligand properties than those of acetonitrile, and, as expected, the peak that we assign to oxidation of B^+ appears only at the lowest scan rates and is almost completely suppressed at 20 V/s which indicates that the rate constant for coordination is about 10 times slower in these solvents as compared to acetonitrile. In each of these solvents, the reduction peaks

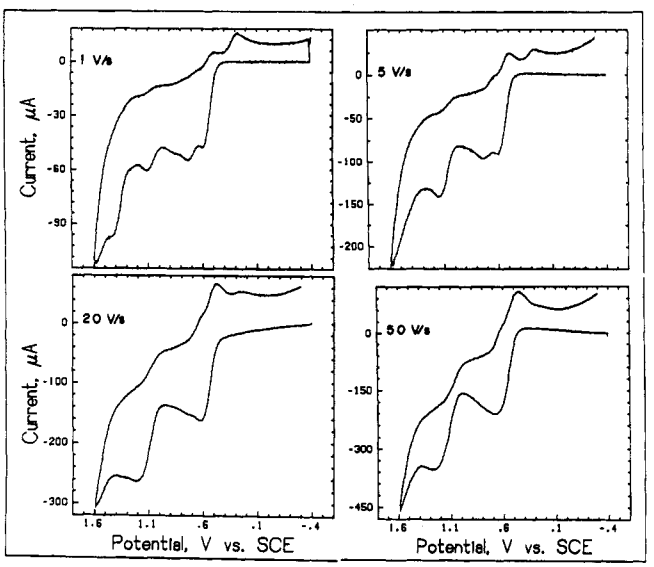

Figure 7. Cyclic voltammograms of 1.0 mM $Mn_2(\mu\text{-}SMe)_2(\mu\text{-}CO)(PMe_3)_2(CO)_4$ in 0.10 M TBAP/CH_2Cl_2 as a function of scan rate.

are smaller than was seen with acetonitrile, suggesting that the cations also undergo irreversible chemical degradation.

Voltammetric results in dichloromethane suggest that this solvent also coordinates to the manganese center. Although coordination of CH_2Cl_2 to a metal center is unusual, it is not unprecedented. Crabtree and co-workers have observed the coordination of halocarbons to iridium hydride complexes. Initially these researchers crystallographically documented the covalent bond between the two iodine atoms and the iridium center in the cation $[IrH_2(o\text{-}C_6H_4I_2)(PPh_3)_2]^+$.[28] In this cation the diiodobenzene acts as a chelating ligand to the metal center. More recently, Crabtree et al. have proposed the coordination of chlorine in another iridium hydride.[29]

In these three dimanganese systems we have observed stepwise oxidation processes that we believe result in a change in the bonding of the metal centers. The recent literature abounds with examples of redox processes which are accompanied by structural changes.[30] Often these redox processes are overall two-electron-transfer reactions in which the second electron is easier to remove or add due to a structural change which has reordered the energetics of the system. If the change in the molecular geometry is small enough or no change occurs, stepwise processes are observed. Zhuang et al. has observed reversible two-electron oxidations in a single step for the similar thiolate-bridged systems $[Et_4N]_2[Mo_2(\mu\text{-}SR)_2(CO)_8]$[31] and $[Et_4N]_2[W_2(\mu\text{-}SR)_2(CO)_8]$[32] (R = Ph, *t*-Bu). They propose the formation of a metal–metal bond and a structural rearrangement to account for the electrochemical behavior. Ginsburg et al.[33] observed a similar two-electron process for the reduction of $Fe_2(CO)_6(\mu\text{-}PPh_2)_2$ to its dianion that was accompanied by a change in the geometry of the core and loss of the metal–metal bond. In the dimanganese systems, the formation of a metal–metal bond must not significantly alter the core geometry allowing the observation of a stepwise removal of electrons.

Conclusion

In the triply and doubly thiolate-bridged dimanganese compounds we suggest the formation of a metal–metal bond which accompanies the removal of an electron from the predominately metal HOMO. This bond formation is supported by ESR spectroscopy, cyclic voltammetry, and chemical reasoning. In the carbonyl-bridged system, the oxidation of $Mn_2(\mu\text{-}SMe)_2(\mu\text{-}CO)(PMe_3)_2(CO)_4$ is followed by a chemical reaction which is thought to be the coordination of solvent to the metal with concomitant conversion of a bridging carbonyl to a terminal position. We have been able to use cyclic voltammetry to probe the kinetics and digital simulation to confirm the mechanism of the solvent addition. By simulating the mechanism we have gained quantitative information about the kinetics of the solvent addition. We are continuing to probe the generality of solvent addition to other carbonyl-bridged metal dimers.

Acknowledgment. We wish to thank Prof. Brock Spencer (Beloit College) for advice and discussions on the ESR spectroscopy and David Kanis for the Fenske–Hall molecular orbital calculation. This research was supported by a grant from the National Science Foundation (CHE-8615255).

Registry No. $Mn_2(\mu\text{-}SMe)_2(\mu\text{-}CO)(PMe_3)_2(CO)_4$, 111555-46-5; $Mn_2(\mu\text{-}SPh)_2(\mu\text{-}CO)(PMe_3)_2(CO)_4$, 111554-36-0; $Mn_2(\mu\text{-}SBu\text{-}t)_2(\mu\text{-}CO)(PMe_3)_2(CO)_4$, 111437-77-5; $Mn_2(\mu\text{-}SMe)_2(\mu\text{-}CO)(PPh_3)_2(CO)_4$, 111437-78-6; $Mn_2(\mu\text{-}SPh)_2(\mu\text{-}CO)(PPh_3)_2(CO)_4$, 111437-79-7; $Mn_2(\mu\text{-}SMe)_2(CO)_8$, 21321-38-0; $Mn_2(\mu\text{-}SPh)_2(CO)_8$, 21240-14-2; $Mn_2(\mu\text{-}SBu\text{-}t)_2(CO)_8$, 111437-80-0; *n*-$Bu_3SnSMe$, 17314-32-8; *n*-$Bu_3SnSPh$, 17314-33-9; $[Mn_2(\mu\text{-}SMe)_3(CO)_6]^-$, 99016-24-7; $Mn_2(\mu\text{-}SMe)_3(CO)_6$, 111437-81-1; $[Mn_2(\mu\text{-}SMe)_3(CO)_6]^+$, 111437-82-2; $[Mn_2(\mu\text{-}S\text{-}t\text{-}Bu)_3(CO)_6]$, 99016-22-5; $Mn_2(\mu\text{-}S\text{-}t\text{-}Bu)_3(CO)_6$, 111437-83-3; $[Mn_2(\mu\text{-}S\text{-}t\text{-}Bu)_3(CO)_6]^+$, 111437-84-4; $[Mn_2(\mu\text{-}SPh)_3(CO)_6]^-$, 96212-28-1; $Mn_2(\mu\text{-}SPh)_3(CO)_6$, 96212-30-5; $[Mn_2(\mu\text{-}SPh)_3(CO)_6]^+$, 96212-31-6; $[Mn_2(\mu\text{-}SCF_3)_3(CO)_6]^-$, 100312-19-4; $Mn_2(\mu\text{-}SCF_3)_3(CO)_6$, 111437-85-5; $[Mn_2(\mu\text{-}SCF_3)_3(CO)_6]^+$, 111437-86-6; $Mn_2(\mu\text{-}SMe)_2(dppm)(CO)_6$, 99016-30-5; $Mn_2(\mu\text{-}SMe)_2(dppm)(CO)_6]^+$, 111437-87-7; $[Mn_2(\mu\text{-}SMe)_2(dppm)(CO)_6]^{2+}$, 111437-88-8; $Mn_2(\mu\text{-}S\text{-}t\text{-}Bu)_2(PMe_3)_2(CO)_6$, 99016-27-0; $[Mn_2(\mu\text{-}S\text{-}t\text{-}Bu)_2(PMe_3)_2(CO)_6]^+$, 111468-57-6; $[Mn_2(\mu\text{-}S\text{-}t\text{-}Bu)_2(PMe_3)_2(CO)_6]^{2+}$, 111437-89-9; $Mn_2(\mu\text{-}S\text{-}t\text{-}Bu)_2(dppm)(CO)_6$, 99016-29-2; $[Mn_2(\mu\text{-}S\text{-}t\text{-}Bu)_2(dppm)(CO)_6]^+$, 111437-90-2; $[Mn_2(\mu\text{-}S\text{-}t\text{-}Bu)_2(dppm)(CO)_6]^{2+}$, 111437-91-3; $Mn_2(\mu\text{-}SPh)_2(dppm)(CO)_6$, 99016-28-1; $[Mn_2(\mu\text{-}SPh)_2(dppm)(CO)_6]^+$, 111437-92-4; $[Mn_2(\mu\text{-}SPh)_2(dppm)(CO)_6]^{2+}$, 111437-93-5; $MnBr(PPh_3)_2(CO)_3$, 14244-44-1; Mn, 7439-96-5; acetonitrile, 75-05-8.

Supplementary Material Available: Tables of anisotropic thermal parameters, interatomic distances, and interatomic angles (3 pages); a listing of observed and calculated structure factors (32 pages). Ordering information is given on any current masthead page.

(28) Crabtree, R. H.; Faller, J. W.; Mellea, M. F.; Quirk, J. M. *Organometallics* **1982**, *1*, 1361.
(29) Crabtree, R. H.; Mellea, M. F.; Quirk, J. M. *J. Am. Chem. Soc.* **1984**, *106*, 2913.
(30) Geiger, W. E. *Prog. Inorg. Chem.*; **1985**; *33*, 275–352.
(31) Zhuang, B.; McDonald, J. W.; Schultz, F. A.; Newton, W. E. *Organometallics* **1984**, *3*, 943.
(32) Zhuang, B.; McDonald, J. W.; Schultz, F. A.; Newton, W. E. *Inorg. Chim. Acta* **1985**, *99*, L29.
(33) Ginsburg, R. E.; Rothrock, R. K.; Finke, R. G.; Collman, J. P.; Dahl, L. F. *J. Am. Chem. Soc.* **1979**, *101*, 6550.